One- and two-electron photoejection from H^-: A multichannel J-matrix calculation

John T. Broad* and William P. Reinhardt†
Department of Chemistry, University of Colorado, Boulder, Colorado 80309
and Joint Institute for Laboratory Astrophysics, University of Colorado and National Bureau of Standards, Boulder, Colorado 80309

(Received 3 August 1976)

The multichannel J-matrix technique is used to solve the pseudostate close-coupling equations for H^- photodetachment using only L^2 basis functions and standard configuration-interaction techniques. The problem of linear dependence which arises when the same L^2 basis is used to expand both the target and free electrons is discussed and exactly solved using a matrix partitioning. Results for total and partial photodetachment cross sections are given from threshold to 70-eV photon energy (1664 to 18 nm) with emphasis on the single-photon two-electron ejection cross section, and the ^1P shape resonance just above the hydrogenic $n = 2$ threshold.

I. INTRODUCTION

Determination of the H^- photodetachment cross section has received considerable experimental and theoretical attention due both to its astrophysical importance and to the fact that it is a manageable, but nontrivial, theoretical exercise. The relative experimental results of Smith and Burch[1] in the visible region of the spectrum have been put on an absolute basis by Geltman,[2(a)] in an analysis of the integrated measurements of Branscomb and Smith.[2(b)] An independent absolute cross section in the same spectral region has recently been obtained by Popp and Kruse.[3] In the uv region Ott, Slater, Cooper, and Gieres[4] have attempted, unsuccessfully, in an initial experiment, to observe the ^1P shape resonance above the hydrogenic $n=2$ threshold via uv photoemission in a local-thermodynamic-equilibrium (LTE) plasma. This shape resonance has been theoretically discussed by Macek[5]; Macek and Burke[6]; Hyman, Jacobs, and Burke[7]; Herrick and Sinanoğlu,[8(a)] and Wulfman,[8(b)] using Lie algebra techniques; and by Lin.[9] It has been observed in electron impact excitation of H atoms by McGowan, Williams, and Curley,[10] and by Williams and Willis.[11]

In the energy region where only the H(1s) final state is energetically accessible the photodetachment cross section has been calculated by, among others, Chandrasekhar,[12] Doughty *et al.*,[13] Bell and Kingston,[14] Macek,[5] Adelman,[15] Kim,[16] Langhoff and Corcoran,[17] Rescigno and McKoy,[18] Ajmera and Chung,[19] and Langhoff *et al.*[20] At energies above the opening of the $n=2$ threshold Macek,[5] using a correlated ground state and a $1s$-$2s$-$2p$ three-state close-coupling final state, has computed the total photodetachment and the partial cross section for excitation of the $n=2$ levels; Hyman, Jacobs, and Burke,[7] again in the three-state close-coupling approximation, have extended this work to determine the σ_{2p}/σ_{2s} branching ratio, which is quite sensitive to final-state coupling. Broad and Reinhardt[21] have used moment techniques to extract the *total* photodetachment cross section over the range of photon energies from threshold to ~60 eV using fully correlated initial and final states.

Risley has recently given a review of H^- photodetachment processes.[22]

In this paper, using the J-matrix formulation[23-27] of close-coupling theory[28] we extend our previous calculation[21] of the total photodetachment cross section to a multichannel analysis resulting in cross sections for the processes

$$\begin{aligned}\hbar\omega + H^- &\rightarrow H(1s) + e^- \\ &\rightarrow H(n=2) + e^- \\ &\rightarrow H^+ + 2e^-\end{aligned}$$

and the total cross section from 0- to 70-eV photon energy.

The close-coupling[28] approach has achieved considerable success in the calculation of many-channel electron-atom scattering and photodetachment cross sections. The recently developed J-matrix method provides a way of reducing the entire set of closely coupled differential equations to matrix equations with square integrable (L^2) basis functions. Heller and Yamani[23] introduced the method with an analysis of s-wave potential scattering (to be referred to as I) and an application to ^1S electron-hydrogen scattering[24] (to be referred to as II). Yamani and Fishman extended I and II to general l, a wider choice of basis sets, and to Coulomb scattering[25] (to be referred to as III), while Broad and Reinhardt developed the full multichannel formalism in the LS coupling scheme[27] (to be referred to as IV). A review of this work,

with emphasis on the application to H^- photodetachment considered here, is given in Sec. II.

In the dipole approximation when the ^1S ground state of H^- absorbs a photon of sufficient energy, one or two electrons can be ejected into continuum states of overall ^1P symmetry. In this work, a manifold of ^1P wave functions is constructed at each energy from the output of a bound-state-type configuration-interaction (CI) program and a subsequent analysis by the J-matrix method. When a basis set spanning the Hilbert space of two-electron bound states appropriate to the CI program is used to describe a multichannel scattering system, where a larger asymptotic Hilbert space is appropriate,[29] a collapse of this larger space occurs. A detailed analysis of the linear dependency causing this collapse and the consequent modification of the solution of the multichannel scattering equations is presented in Sec. III A, with a qualitative discussion in Sec. III B. The form of the one-electron photodetachment cross section is given in Sec. III C, and in Sec. III D the *equivalent-quadrature*[30,31] construction of the cross section for two-electron ejection is pursued.

Section IV describes the details of the computation based on the theory of Sec. II and III, while Sec. V contains the resulting cross sections. Qualitatively correct resonance phenomena are seen at the inelastic thresholds, the oscillator strength for excitation to the ^1P shape resonance just above the $n=2$ threshold is discussed, and an estimate of the total two-electron ejection cross section converged to ~15% is obtained.

II. REVIEW OF J-MATRIX THEORY

A. Potential scattering

The basis of the J-matrix method (I,III) is that in the complete set of nonorthogonal Laguerre functions

$$\phi_n(\lambda r) = (\xi r)^{l+1} e^{-\xi r/2} L_n^{2l+1}(\xi r), \quad n = 0, 1, 2\ldots \tag{2.1}$$

the matrix elements of $H_0 - E$ for

$$H_0 = -\frac{1}{2}\frac{d^2}{dr^2} + \frac{l(l+1)}{2r^2} + \frac{Z}{r} \tag{2.2}$$

are of tridiagonal, or Jacobi, form:

$$J_{nm}(k) \equiv \int_0^\infty dr\, \phi_n(\xi r)[H_0 - k^2/2]\phi_m(\xi r)$$
$$= \Gamma(n+2l+2)/\Gamma(n+1)\{Z\delta_{nm} - \xi\eta/(2\sin\theta)[2x(n+l+1)\delta_{m,n} - n\delta_{m,n-1} - (n+2l+2)\delta_{m,n+1}]\}, \tag{2.3}$$

where $\eta = k/\xi$ and $x = \cos\theta = (\eta^2 - \frac{1}{4})/(\eta^2 + \frac{1}{4})$. We limit further discussion to the case $Z = 0$ appropriate to the photoionization of a singly charged negative ion. As shown in I and III, it is possible to exploit the tridiagonal nature of $H_0 - k^2/2$ in the Laguerre basis to solve the infinite set of matrix equations for the expansions of two independent solutions to the Schrödinger equation. The regular solution

$$\bar{S}(r) = \sum_{n=0}^{\infty} \phi_n(\xi r) s_n(\eta) \tag{2.4}$$

is, for $Z = 0$, the Ricatti Bessel function $(kr)j_l(kr)$ having expansion coefficients

$$s_n(\eta) = \frac{2^l \Gamma(l+1)}{\Gamma(2l+2)}(\sin\theta)^{l+1} \times {}_2F_1(-n, n+2l+2, \tfrac{1}{2}, \sin^2\tfrac{1}{2}\theta)\,. \tag{2.5}$$

The other function,

$$\bar{C}(r) = \sum_{n=0}^{\infty} \phi_n c_n(\eta), \tag{2.6}$$

is a solution of the inhomogeneous equation

$$(H_0 - k^2/2)\bar{C}(r) = k/2 s_0 \bar{\phi}_0(\xi r), \tag{2.7}$$

where $\langle \bar{\phi}_0 | \phi_n \rangle = \delta_{n0}$. $\bar{C}(r)$ can be shown to be a sum of a Ricatti Neumann function $(kr)n_l(kr)$ and $e^{-\xi r/2} r^{-l}$ times a polynomical of degree $2l$ of such a form that $\bar{C}(r) \to r^{l+1}$ as $r \to 0$. As shown in III, Eqs. (2.6) and (2.7) lead to

$$c_n(\eta) = -\frac{2^l \Gamma(l+\frac{1}{2})\Gamma(n+1)}{\sqrt{\pi}\,\Gamma(n+2l+2)(\sin\theta)^l} \times {}_2F_1(-n-2l-1, n+1; \tfrac{1}{2}-l; \sin^2\tfrac{1}{2}\theta)\,. \tag{2.8}$$

Since the hypergeometric functions in Eqs. (2.5)–(2.8) each have one negative-integer index, they reduce to easily calculable polynomials.

At large r,

$$\bar{S}(r) \to \sin(kr - l\pi/2), \quad \bar{C}(r) \to \cos(kr - l\pi/2). \tag{2.9}$$

The solution of potential scattering problems using these asymptotically correct solutions is discussed in detail in I–III, while the general multichannel analysis of electron-atom scattering in the L-S coupling scheme is given in IV. We restrict our attention here to the formulation and solution of the many-channel close-coupling equations for the electron-hydrogen scattering problem needed to describe the final state in the photodetachment of H^-.

B. Multichannel scattering in L-S coupling

Let the target hydrogen atom be described by a finite set of orthonormal radial wave functions $\chi_\nu^\lambda(\rho)$, $\nu=0,1,\ldots,N_\lambda$, obtained numerically by diagonalizing the Coulomb Hamiltonian in a finite basis such that

$$\int_0^\infty d\rho\,\chi_{\nu'}^\lambda\left(-\frac{1}{2}\frac{d^2}{d\rho^2}+\frac{\lambda(\lambda+1)}{2\rho^2}-\frac{1}{\rho}\right)\chi_\nu^\lambda=\epsilon_{\nu\lambda}\delta_{\nu'\nu}. \tag{2.10}$$

The first few of these matrix eigenfunctions of each angular symmetry will have energies close to the correct hydrogenic values of $-1/2(\nu+\lambda+1)^2$. The remaining ones, some of which will have positive eigenvalues, function as pseudostates.[31,32]

The target radial wave functions of Eq. (2.10) are combined with spherical harmonics to generate a channel function of the target coordinate $\vec{\rho}$ and the free-electron angular coordinate $\hat{r}$ with desired total angular momenta L,M:

$$\begin{aligned}\chi_\Gamma(\vec{\rho},\hat{r})&=\chi_\nu^\lambda(\rho)\mathcal{Y}_{\lambda lLM}(\hat{\rho},\hat{r})\\&=\chi_\nu^\lambda(\rho)\sum_{m\mu}C(l\lambda L,m\mu M)Y_{lm}(\hat{r})Y_{\lambda\mu}(\hat{\rho}),\end{aligned} \tag{2.11}$$

where C is the Clebsch-Gordan coefficient combining Y_{lm} and $Y_{\lambda\mu}$ into the double spherical harmonic $\mathcal{Y}_{\rho\lambda LM}$, and $\Gamma=\{\nu,\lambda,l,LM\}$ designates the channel.

To complete the designation of a basis, there remains only the specification of the radial wave function for the free electron, and it is here that the division between an inner and an outer region of function space characteristic of the J-matrix method is introduced. Following Eq. (2.1), the outer ($n\geq N_\Gamma$) radial functions are taken to be

$$\phi_n^\Gamma(\xi_\Gamma r)=(\xi_\Gamma r)^{l+1}e^{-\xi_\Gamma r/2}L_n^{2l+1}(\xi_\Gamma r). \tag{2.12}$$

The inner, or coupled, radial functions are then chosen as an orthonormal linear combinations of the ϕ_n^Γ for $n<N_\Gamma$:

$$\psi_n^\Gamma(r)=\sum_{p=0}^{N_\Gamma-1}\phi_p^\Gamma(\xi_\Gamma r)D_{pn}^\Gamma. \tag{2.13}$$

Together, the inner and outer functions, Eqs. (2.12) and (2.13), constitute a complete basis in the coordinate of the free electron, r, for each channel Γ, and the number of inner functions N_Γ determines the accuracy with which the full potential will be described. Combining (2.11) with (2.12), (2.13) gives the full two-electron functions (for singlets)

$$\Phi_n^\Gamma(\vec{\rho},\vec{r})=\frac{1+P}{\sqrt{2}}\begin{cases}\chi_\Gamma(\vec{\rho},\hat{r})\psi_n^\Gamma(r), & n=0,1,\ldots N_\Gamma-1\\ \chi_\Gamma(\vec{\rho},\hat{r})\phi_n^\Gamma(r), & n=N_\Gamma,N_\Gamma+1,\ldots,\infty\end{cases} \tag{2.14}$$

where P acts to permute the coordinates of the two electrons. As will become clear in Sec. III, the two-electron functions ϕ_n^Γ of Eq. (2.14) constitute an overcomplete basis in the two-electron Hilbert space usually considered in bound-state calculations. In fact, the Φ_n^Γ constitute a basis for a larger, asymptotic Hilbert space consisting of a direct sum of channel subspaces[29] appropriate to the system under consideration.

The full scattering wave function can be expanded in terms of the Φ_n^Γ as

$$\Theta_\Gamma(\vec{\rho},\vec{r};E)=\sum_{\Gamma'}\left(\sum_{n'=0}^{N_{\Gamma'}-1}\Phi_{n'}^{\Gamma'}a_{n'}^{\Gamma'\Gamma}+\sum_{n'=N_{\Gamma'}}^{\infty}\Phi_{n'}^{\Gamma'}f_{n'}^{\Gamma'\Gamma}\right), \tag{2.15}$$

where the $a_{n'}^{\Gamma'\Gamma}$ are unknown expansion coefficients of the inner ($n'<N_{\Gamma'}$) portion of the wave function and the coefficients of the outer ($n'\geq N_{\Gamma'}$) portion, $f_{n'}^{\Gamma'\Gamma}$, are expressed below. If the channel Γ' is open, or $k_{\Gamma'}^2/2\equiv E-\epsilon_{\nu\lambda}>0$,

$$f_{n'}^{\Gamma'\Gamma}=[2/(\pi k_{\Gamma'})]^{1/2}\{s_{n'}(\eta_{\Gamma'})\delta_{\Gamma'\Gamma}+c_{n'}(\eta_{\Gamma'})R_{\Gamma'\Gamma}\}, \tag{2.16}$$

where $\eta_{\Gamma'}=k_{\Gamma'}/\zeta_{\Gamma'}$ and $R_{\Gamma'\Gamma}$ is the unknown reactance matrix. For closed channels, with $k_{\Gamma'}^2/2<0$,

$$f_{n'}^{\Gamma'\Gamma}=[2/(\pi k_{\Gamma'})]^{1/2}\{c_{n'}(\eta_{\Gamma'})+is_{n'}(\eta_{\Gamma'})\}R_{\Gamma'\Gamma}, \tag{2.17}$$

where, again, $R_{\Gamma'\Gamma}$ is unknown. Thus by Eqs. (2.5), (2.8), (2.9), and (2.16), the sum over open channels Γ' contributes terms of asymptotic form $\sin(k_{\Gamma'}r-l'\pi/2)\delta_{\Gamma'\Gamma}+\cos(k_{\Gamma'}r-l'\pi/2)R_{\Gamma'\Gamma}$ to the wave function, while the sum over closed channels includes the expansion coefficients c_n+is_n of the Ricatti Hankel-function-like solution to the inhomogeneous equation (2.7), and thereby contributes terms which die exponentially at large r. The addition of these closed-channel terms speeds convergence of calculations at energies just below thresholds.[24]

The unknown $a_{n'}^{\Gamma'\Gamma}$ and $R_{\Gamma'\Gamma}$ are determined by requiring that

$$\langle\Phi_{n''}^{\Gamma''}\,|\,(H-E)^{(N)}\,|\,\Theta_\Gamma\rangle=0,\quad n''=0,1,\ldots,\infty,\quad \Gamma''\sim\text{all channels} \tag{2.18}$$

where H is the sum of the hydrogen Hamiltonian in $\vec{\rho}$, the kinetic energy of the free electron, and the remaining potential energy:

$$H=H_t(\vec{\rho})+H_0(\vec{r})+V(\vec{\rho},\vec{r}), \tag{2.19}$$

$$V(\vec{\rho},\vec{r})=-1/r+1/|\vec{r}-\vec{\rho}|. \tag{2.20}$$

The superscript (N) in Eq. (2.18) indicates that the potential in Eq. (2.20) and all the exchange elements of H in Eq. (2.19) are to be neglected in all

matrix elements with outer ($n \geq N_\Gamma$) functions. Without exchange and without the potential, these matrix elements are immediately reduced to the tridiagonal form of Eq. (2.3); for example,

$$\langle \chi_{\Gamma''} \phi^{\Gamma''}_{n''} \left| H_t + H_0 - E \right| \chi_{\Gamma'} \psi^{\Gamma'}_{n'} \rangle = \delta_{\Gamma''\Gamma'} \sum_{p=0}^{N_{\Gamma'}-1} J_{n''p}(k_{\Gamma'}) D^{\Gamma'}_{pn'}$$

$$n'' \geq N_{\Gamma''}, \quad n' < N_{\Gamma'}. \quad (2.21)$$

As shown in IV the tridiagonal form of J in Eq. (2.3) and the choice of expansion coefficients s_n in Eq. (2.5) and c_n in Eq. (2.8) assure that the infinite set of equations (2.18) is satisfied by construction for $n'' \geq N_{\Gamma''}+1$ and $n' \geq N_{\Gamma'}+1$ in Eq. (2.15). The remaining equations for $n'' \leq N_{\Gamma''}$ and $n' \leq N_{\Gamma'}$ are just sufficient to solve for the unknown $a^{\Gamma'\Gamma}_{n'}$ and $R_{\Gamma'\Gamma}$:

$$\sum_{\Gamma'} \sum_{n'=0}^{N_{\Gamma'}-1} (H-E)^{\Gamma''\Gamma'}_{n''n'} a^{\Gamma'\Gamma}_{n'} + D^{\Gamma''}_{N_{\Gamma''}-1,n''} J^{\Gamma''}_{N_{\Gamma''}-1} f^{\Gamma''\Gamma}_{N_{\Gamma''}} = 0, \quad (2.22)$$

$$\sum_{n'=0}^{N_{\Gamma'}-1} D^{\Gamma''}_{N_{\Gamma''}-1,n'} a^{\Gamma'\Gamma}_{n'} - f^{\Gamma''\Gamma}_{N_{\Gamma''}-1} = 0, \quad (2.23)$$

$n'' = 0, 1, \ldots, N_{\Gamma''}-1$, $\Gamma', \Gamma'' \sim$ all channels, $\Gamma \sim$ open channels.

In IV, it was shown that these equations can be solved by eliminating $a^{\Gamma'\Gamma}_{n'}$ from Eq. (2.23), by construction of $(H-E)^{-1}$, followed by solving for the reactance matrix via Eqs. (2.16) and (2.17).

III. APPLICATION TO H^- PHOTOIONIZATION

A. Collapse of asymptotic Hilbert space

When the hydrogen negative ion in its ^1S ground state absorbs a photon, the only excited states that can be reached in the dipole approximation must be of ^1P symmetry. For this total $L=1$, the rules of angular momentum addition allow only the two possibilities $l = \lambda \pm 1$. To minimize the complexity of the calculation, it was desirable to choose the inner functions for the free electron, ψ^Γ_n, identical to the target hydrogen-atom eigenfunctions χ^Γ_n. This was accomplished by expanding the target hydrogen-atom states χ^λ_ν in the basis functions ϕ^Γ_n, as in Eq. (2.13), and generating the expansion coefficients D^Γ_{pn} so as to diagonalize the hydrogen Hamiltonian, as in Eq. (2.10). As a consequence, the exponent ξ_Γ can no longer depend on ν, λ, and hence, in Eqs. (2.12) and (2.13), ϕ^Γ_n and D^Γ_{pn} are reindexed as ϕ^l_n and D^Γ_{pn}, while ψ^Γ_n and χ^λ_ν can be written as ψ^l_n and ψ^λ_ν. In addition, the number of inner space functions in each channel N_Γ now only depends on l, and can be written as N_l, identical with the number of pseudostates of angular symmetry l.

There are more serious changes than mere reindexing, however. When the inner basis functions in (2.14) are

$$\phi^\Gamma_n = (1+P)/\sqrt{2}\, \psi^\lambda_\nu(\rho) \psi^l_n(r) \mathcal{Y}_{\lambda l L M}(\hat{\rho}, \hat{r}), \quad (3.1a)$$

then

$$\Phi^{\nu\lambda l}_n = \Phi^{nl\lambda}_\nu, \quad (3.1b)$$

implying that the quantum numbers ν, λ of the target-atom electron can be exchanged with the quantum numbers n, λ of the free electron without changing the wave function. It will be useful to designate the set of numbers $\{n, l, \lambda\}$ as Γ_{ex} in analogy to $\Gamma \equiv \{\nu, \lambda, l\}$.

As a consequence of (3.1b), the matrix elements of $(H-E)$ exhibit symmetry under exchange of the free and target quantum numbers:

$$(H-E)^{\Gamma'\Gamma}_{n'n} = (H-E)^{\Gamma'_{ex}\Gamma}_{\nu' n} = (H-E)^{\Gamma'\Gamma_{ex}}_{n'\nu} = (H-E)^{\Gamma'_{ex}\Gamma_{ex}}_{\nu'\nu}. \quad (3.2)$$

It is then natural to split $(H-E)$ into four blocks according to $l' = \lambda' \pm 1$, $l = \lambda \pm 1$:

$$(H-E) = \begin{pmatrix} (H-E)_{++} & (H-E)_{+-} \\ (H-E)_{-+} & (H-E)_{--} \end{pmatrix}. \quad (3.3)$$

To make this more explicit, consider a ^1P calculation consisting of only the four orbitals, $1s, 2s, 2p, 3p$. For this illustration, we will place the indices on $(H-E)$ in a way more conventional for configuration-interaction calculations by denoting, for example,

$$(H-E)^{\Gamma'\Gamma}_{n'n} = (H-E)_{1s2p,1s2p}, \quad \Gamma' = \{1s, p\},\ n' = 2 \text{ and } \Gamma = \{1s, p\},\ n = 2. \quad (3.4)$$

In Eq. (3.4), the target quantum numbers ν, λ are written first, followed by the free-electron angular momentum l and expansion-function number n. In the ++ block of $(H-E)$ $\lambda' = l'+1$ and $\lambda = l+1$, or in this example the target is in an s state and the free electron in a p state, yielding

$$(H-E)_{++} = \begin{bmatrix} H_{1s2p,1s2p}-E & H_{1s2p,1s3p} & H_{1s2p,2s2p} & H_{1s2p,2s3p} \\ H_{1s3p,1s2p} & H_{1s3p,1s3p}-E & H_{1s3p,2s2p} & H_{1s3p,2s3p} \\ H_{2s2p,1s2p} & H_{2s2p,1s3p} & H_{2s2p,2s2p}-E & H_{2s2p,2s3p} \\ H_{2s3p,1s2p} & H_{2s3p,1s3p} & H_{2s3p,2s2p} & H_{2s3p,2s3p}-E \end{bmatrix}. \quad (3.5)$$

In the $--$ block, on the other hand, $\lambda' = l' - 1$ and $\lambda = l - 1$ or, in this example, the target is in a p state and the free electron in an s state:

$$(H-E)_{--} = \begin{pmatrix} H_{2p1s,2p1s}-E & H_{2p1s,2p2s} & H_{2p1s,3p1s} & H_{2p1s,3p2s} \\ H_{2p2s,2p1s} & H_{2p2s,2p2s}-E & H_{2p2s,3p1s} & H_{2p2s,3p2s} \\ H_{3p1s,2p1s} & H_{3p1s,2p2s} & H_{3p1s,3p1s}-E & H_{3p1s,3p2s} \\ H_{3p2s,2p1s} & H_{3p2s,2p2s} & H_{3p2s,3p1s} & H_{3p2s,3p2s}-E \end{pmatrix} . \tag{3.6}$$

Note how the rows and columns in Eqs. (3.5) and (3.6) are ordered so that the target quantum number ν changes more slowly than n. The off-diagonal blocks in Eq. (3.3) have the appropriate mixed ordering $\lambda' = l \pm 1$, $\lambda = l \mp 1$.

According to Eq. (3.2), however, $H_{1s2p,1s3p}$ in Eq. (3.5) equals $H_{2p1s,3p1s}$ in Eq. (3.6), for example; hence the four blocks of $(H-E)$ are merely reorderings of each other. This linear dependence among the elements implies that the full matrix $(H-E)$ is singular. A study of this singularity reveals a way of solving the scattering equations.

Equation (3.2) gives a relation among the blocks of $(H-E)$. For example,

$$[(H-E)_{+-}]^{\Gamma'\Gamma}_{n'n} = \sum_{\substack{\lambda'' \\ l''=\lambda''+1}} \sum_{\nu'' n''} [(H-E)_{++}]^{\Gamma'\Gamma''}_{n'n''} V^{\Gamma''\Gamma}_{n''n}$$

$$= [(H-E_{++}]^{\Gamma'\Gamma}_{n'\nu} {}^{\rm ex} , \tag{3.7}$$

where V is a matrix which reorders the indices:

$$V^{\Gamma'\Gamma}_{n'n} = \delta_{\Gamma' n', \Gamma_{\rm ex}\nu} . \tag{3.8}$$

Similarly for the other blocks in Eq. (3.3),

$$(H-E) = \begin{pmatrix} (H-E)_{++} & (H-E)_{++}V \\ (H-E)_{--}V^{\dagger} & (H-E)_{--} \end{pmatrix}$$

$$= \begin{pmatrix} (H-E)_{++} & 0 \\ 0 & (H-E)_{--} \end{pmatrix} \begin{pmatrix} I_+ & V \\ V^{\dagger} & I_- \end{pmatrix} = [\mathcal{H}-\mathcal{E}]\Xi \tag{3.9}$$

where the definitions of $[\mathcal{H}-\mathcal{E}]$ and Ξ are apparent. Writing

$$\Xi = \begin{pmatrix} I_+ & 0 \\ V^{\dagger} & 0 \end{pmatrix} \begin{pmatrix} I_+ & V \\ 0 & 0 \end{pmatrix} , \tag{3.10}$$

it is clear that Ξ is singular. Since $[\mathcal{H}-\mathcal{E}]$ is composed of two nonsingular blocks on the diagonal, it is evident that the singularity in $(H-E)$ is due entirely to that of Ξ.

It is not possible, then, to solve (2.22) for the coefficients $a^{\Gamma'\Gamma}_{n'}$ by inverting $(H-E)$, but a look at the scattering wave function (2.15) reveals that full knowledge $a^{\Gamma'\Gamma}_{n'}$ is not required. Splitting the matrix of coefficients a into blocks in the same way as $(H-E)$,

$$a = \begin{pmatrix} a_{++} & a_{+-} \\ a_{-+} & a_{--} \end{pmatrix} , \tag{3.11}$$

and designating the inner space sum in (2.15) as $\theta^{\rm inner}_{\Gamma}$, yields for $l = \lambda + 1$,

$$\theta^{\rm inner}_{\Gamma} = \sum_{\substack{\lambda'\nu'n' \\ l'=\lambda'+1}} \Phi^{\Gamma'}_{n'} (a_{++})^{\Gamma'\Gamma}_{n'} + \sum_{\substack{\lambda'\nu'n' \\ l'=\lambda'-1}} \Phi^{\Gamma'}_{n'} (a_{-+})^{\Gamma'\Gamma}_{n'}$$

$$= \sum_{\substack{\lambda'\nu'n' \\ l'=\lambda+1}} \Phi^{\Gamma'}_{n'} [a_{++} + V a_{-+}]^{\Gamma'\Gamma}_{n'} . \tag{3.12}$$

Thus for $l = \lambda + 1$, only the combination $(a_+)^{\Gamma'\Gamma}_{n'} = (a_{++})^{\Gamma'\Gamma}_{n'} + (Va_{-+})^{\Gamma'\Gamma}_{n'}$ is needed. Likewise, for $l = \lambda - 1$, only $(a_-)^{\Gamma'\Gamma}_{n} = (Va_{+-})^{\Gamma'\Gamma}_{n} + (a_{--})^{\Gamma'\Gamma}_{n}$ is required, or in matrix form, using the definition of Ξ in Eq. (3.12),

$$\Xi a = \begin{pmatrix} I_+ & V \\ V^{\dagger} & I_- \end{pmatrix} \begin{pmatrix} a_{++} & a_{+-} \\ a_{-+} & a_{--} \end{pmatrix} = \begin{pmatrix} a_+ & Va_- \\ V^{\dagger}a_+ & a_- \end{pmatrix} . \tag{3.13}$$

Thus, by Eqs. (3.9) and (3.12),

$$(H-E)a = [\mathcal{H}-\mathcal{E}](\Xi a) , \tag{3.14}$$

and since $[\mathcal{H}-\mathcal{E}]$ can be inverted, Eq. (2.22) could be solved for (Ξa). The fact that there are only two independent blocks of coefficients a_+, a_- is directly related to the singularity of $(H-E)$.

The program can be completed by noticing that the choice of identical target and inner functions allows the effect of exchange to be included exactly in the matrix elements of $(H_t + H_0 - E)$ between inner and outer functions in Eq. (2.18). The equations to be solved instead of (2.22), (2.23) are then

$$\sum_{\Gamma'} \sum_{n'=0}^{N_{l'}-1} (H-E)^{\Gamma''\Gamma'}_{n''n'} a^{\Gamma'\Gamma}_{n'} + D^{l''}_{N_{l''-1},n''} J^{\Gamma''}_{N_{l''-1},N_{l''}} f^{\Gamma''\Gamma}_{N_{l''}}$$

$$+ D^{\lambda''}_{N_{\lambda''-1},\nu''} J^{\Gamma''_{\rm ex}}_{N_{\lambda''-1},N_{\lambda''}} f^{\Gamma''_{\rm ex}}_{N_{\lambda''}} = 0 ,$$

$$n'' = 0, 1, \ldots, N_{l''} - 1 \tag{3.15}$$

$$\sum_{n'=0}^{N_{l''}-1} D^{l''}_{N_{l''-1},n'} a^{\Gamma''\Gamma}_{n'} + \sum_{\nu'=0}^{N_{\lambda''-1}} D^{\lambda''}_{N_{\lambda''-1},\nu'} a^{\Gamma''_{\rm ex}\Gamma}_{\nu'} - f^{\Gamma''\Gamma}_{N_{l''-1}} = 0 . \tag{3.16}$$

By using the matrix definitions (3.9), (3.11) and defining

$$(D)^{\Gamma''\Gamma'}_{n'} = D^{l''}_{N_{l''-1},n'} \delta_{\Gamma''\Gamma'} + D^{l''}_{N_{l''-1},\nu'} \delta_{\Gamma''\Gamma'_{\rm ex}} , \tag{3.17}$$

$$(J)^{\Gamma''\Gamma'} = J^{\Gamma''}_{N_{l''-1},N_{l''}}\delta_{\Gamma''\Gamma'}, \quad (F_N)^{\Gamma''\Gamma} = f^{\Gamma''\Gamma}_{N_{l''}} \ . \quad (3.18)$$

Equations (3.15), (3.16) can be written as matrix equations

$$(H-E)a + DJF_N = 0 \ , \quad (3.19)$$

$$Da - F_{N-1} = 0 \ . \quad (3.20)$$

By further defining $(D_\pm)^{\Gamma''\Gamma'}_{n'} = D^{l''}_{N_{l''-1},n'}\delta_{\Gamma''\Gamma'}$ for $l'' = \lambda'' \pm 1$ and $l' = \lambda' \pm 1$, it can be seen that

$$D = \begin{pmatrix} D_+ & D_+V \\ D_-V^\dagger & D_- \end{pmatrix} = \begin{pmatrix} D_+ & 0 \\ 0 & D_- \end{pmatrix}\Xi = \mathfrak{D}\Xi \ , \quad (3.21)$$

which defines $\mathfrak{D}$.

Using Eqs. (3.13) and (3.14) in Eqs. (3.18), (3.19), we find

$$[\mathcal{H} - \mathcal{E}]\Xi a + \mathfrak{D}\Xi JF_N = 0 \quad (3.22)$$

and thus

$$\mathfrak{D}\Xi a - F_{N-1} = 0 \ . \quad (3.23)$$

Now Eq. (3.22) can be used to eliminate Ξa from (3.23) and the system of equations solved in a fashion analogous to the general multichannel case discussed below Eqs. (2.12), (2.13). Using Eqs. (2.16), (2.17), and (3.18), the result is the reactance matrix

$$R_{\Gamma'\Gamma} = -\{(\overline{W}CJC)^{-1}(\overline{W}SJS)\}_{\Gamma'\Gamma} \ , \quad (3.24)$$

where

$$\overline{W}SJS_{\Gamma'\Gamma} = [\overline{W}_{\Gamma'\Gamma}J^{\Gamma}_{N_{l}-1,N_l}s_{N_l}(\eta_\Gamma) + \delta_{\Gamma'\Gamma}s_{N_l-1}(\eta_\Gamma)]/(\pi k_\Gamma/2)^{1/2} \ , \quad (3.25)$$

$$\overline{W}CJC_{\Gamma'\Gamma} = (\overline{W}_{\Gamma'\Gamma}J^{\Gamma}_{N_{l}-1,N_l}c_{N_l}(\eta_\Gamma) + \delta_{\Gamma'\Gamma}c_{N_l-1}(\eta_\Gamma))/(\pi k_\Gamma/2)^{1/2} \ , \quad (3.26)$$

$$\overline{W}_{\Gamma'\Gamma} = (\mathfrak{D}[\mathcal{H} - \mathcal{E}]^{-1}\Xi\mathfrak{D}^\dagger)_{\Gamma'\Gamma} \ . \quad (3.27)$$

In line with Eqs. (2.16), (2.17), the channel index in Eqs. (3.24) and (3.26) runs only over open channels while all the other channel indices run over all channels, open and closed. When Γ is a closed channel in Eq. (3.26) the coefficients c^Γ_n are to be evaluated as $c^\Gamma_n + is^\Gamma_n$ as in Eq. (2.17). The analogy between the form of Eq. (3.27) and the matrix first formulated by Wigner[33] and used in R-matrix theory[34] to match the solutions between inner and outer regions of configuration space has been discussed in IV.

As in the general multichannel case discussed in IV, much of the work of forming $\overline{W}$ and $a_\pm$ can be carried out once for all energies. If H_{++} is diagonalized by the bound state CI program, then $(H-E)^{-1}_{++}$ can be written as

$$[(H-E)^{-1}_{++}]_{ij} = \sum_k \frac{U_{ik}U^\dagger_{kj}}{E_k - E} \ , \quad (3.28)$$

where U is the unitary matrix which diagonalizes the H_{++}, i and j index two-electron configurations with the implicit ordering $l = \lambda + 1$, and k runs over the eigenfunctions of H in the finite basis. Equation (3.27) can then be rewritten as

$$\overline{W}_{\Gamma'\Gamma} = \sum_k \frac{(DU)^{\Gamma'}_k(DU)^{\Gamma}_k}{E_k - E} \ , \quad (3.29)$$

where, using the definition of D_+ and D_- below Eq. (3.20),

$$(DU)^\Gamma_k = \begin{cases} \sum_{n=0}^{N_l-1} D_{N_l-1,n}U_{i(\nu\lambda ln),k} & \text{if } l = \lambda + 1 \\ \sum_{n=0}^{N_l-1} D_{N_l-1,n}U_{i(nl\lambda\nu),k} & \text{if } l = \lambda - 1 \ . \end{cases} \quad (3.30)$$

The notation $i(\nu\lambda ln)$ in (3.30) denotes the one-to-one mapping from two-electron configurations i to the multichannel quantum numbers $\{\nu,\lambda,l,n\}$ for the case $l = \lambda + 1$.

Thus, once DU is known, the reactance matrix can be formed at each energy by Eq. (3.2) with only a channel-by-channel inversion of $\overline{W}CJC$ in addition to finite matrix multiplications and the straightforward calculation of the expansion coefficients c_n and s_n. The proof of the symmetry of the open portion of the reactance matrix given in the Appendix in IV carries over directly for the modified form of $\overline{W}$ in Eq. (3.27).

In the same way as for $\overline{W}$, the inner portion of the scattering wave function in Eq. (3.12) can be expressed as a sum over configurations with the implicit ordering $l = \lambda + 1$:

$$\theta^{\text{inner}}_\Gamma = \sum_i \Phi_i \alpha^\Gamma_i \ , \quad (3.31)$$

where by Eqs. (3.12) and (3.27)

$$\alpha^\Gamma_{i(\nu'\lambda' l'n')} = \begin{cases} (a_+)^{\Gamma\Gamma}_{n'} & \text{if } l = \lambda + 1 \\ (a_-)^{\Gamma'ex\Gamma}_{\nu'} & \text{if } l = \lambda - 1 \end{cases}$$

$$= -\sum_k \sum_{\Gamma''} \frac{U_{ik}(DU)^{\Gamma''}_k}{E_k - E}(JF_N)^{\Gamma''\Gamma} \ . \quad (3.32)$$

As shown in IV [Eq. (3.22)], JF_N can be simplified, by using the properties of the s_n and c_n, to

$$(JF_N)^{\Gamma''\Gamma} = -(1/\pi)(\overline{W}CJC)^{-1}_{\Gamma\Gamma''} \ . \quad (3.33)$$

B. Discussion

The above analysis shows that it is indeed feasible to pursue the multichannel J-matrix method even if the inner and target basis functions are identical. The advantages of this choice can be seen from the form of $[\mathcal{H} - \mathcal{E}]^{-1}$ and its use in Eq. (3.27), for, by Eq. (3.9),

$$[\mathcal{H}-\mathcal{E}]^{-1}=\begin{pmatrix}(H-E)^{-1}_{++} & 0\\ 0 & V^{\dagger}(H-E)^{-1}_{++}V\end{pmatrix}. \tag{3.34}$$

Since for ^1P symmetry, the full matrix $[\mathcal{H}-\mathcal{E}]$ has twice as many rows and columns as the ++ or −− block, only having to invert $(H-E)_{++}$ means a considerable savings in computational effort. Furthermore, H_{++} can be formed and diagonalized by a normal bound-state configuration-interaction program and the results used advantageously as discussed with Eqs. (3.28)–(3.30).

For two-electron symmetries other than ^1P, the rule $l=\lambda\pm1$ does not hold but an analogous analysis of the collapse of the asymptotic Hilbert space into the usual two-electron Hilbert space could be made. For systems containing more than two electrons, on the other hand, the flexibility of varying the free-electron basis exponent ξ_Γ for different target states may make working with the full asymptotic basis more desirable.

C. One-electron photoionization cross section

The cross section for one-electron photodetachment from the ground state of H^- into channel Γ was given in IV as

$$\Gamma_{\sigma_{\rm vel}}(E)=(4\pi^2/\omega c)\left|\langle {}^{\Gamma}\theta_-(E)\left|\nabla\right|\Phi_{\rm gnd}\rangle\right|^2, \tag{3.35a}$$

$$\Gamma_{\sigma_{\rm length}}(E)=(4\pi^2\omega/c)\left|\langle {}^{\Gamma}\theta_-(E)\left|r\right|\Phi_{\rm gnd}\rangle\right|^2 \tag{3.35b}$$

in the velocity and length forms,[35] where ${}^{\Gamma}\theta_-$ is the incoming scattering wave function related to the standing wave θ_Γ by

$$\Gamma_{\theta_-}=-i\sum_{\substack{\Gamma\Gamma'\\ \text{open}}}\theta_{\Gamma'}(1+iR)^{-1}_{\Gamma'\Gamma}. \tag{3.36}$$

The ^1S ground state $\Phi_{\rm gnd}$ can be calculated with a configuration-interaction program and the dipole matrix elements with the inner portion of the sum (2.15) computed over the eigenfunctions of H with the aid of Eqs. (3.31) and (3.33).

D. Two-electron photoionization cross section: $\hbar\omega+H^-\rightarrow H^+ +2e^-$

When the total energy reaches zero, channels with two free final-state electrons open up, and we have to investigate how the channels describing one free electron of energy $E-\epsilon_{\nu\lambda}$ leaving behind a pseudostate of energy $\epsilon_{\nu\lambda}>0$ represent an approximation to this two-electron process.

The total cross section for emitting two electrons from H^- can be shown to be[25]

$$\sigma^{2e^-}_{\rm length}=\frac{4\pi^2\omega}{c}\int\int dE_2\,dE_1\,\delta(E-E_2-E_1)\times\sum_{\lambda l}\left|\langle {}^{\lambda l}\Psi_-(E_2,E_1)\left|r\right|\Phi_{\rm gnd}\rangle\right|^2, \tag{3.37}$$

where ${}^{\lambda l}\Psi(E_2,E_1)$ is a wave function for one electron of angular momentum λ and continuous energy E_2 and another of angular momentum l and continuous energy E_1. Since there are three Coulomb centers, the potential felt by each electron is not well defined in terms of a free electron interacting with a neutral target, but the following reasonable choice can be made in conjunction with the Pauli principle. Since the two emitted electrons are indistinguishable, it is necessary to avoid double counting in (3.37), and one way to do this is to require that $E_1>E_2$ in the integral. Using the δ function under this restriction to do the integral over dE_1 yields

$$\sigma^{2e^-}_{\rm length}(E)=\frac{4\pi^2\omega}{c}\int_0^{E/2}dE_2\times\sum_{\lambda l}\left|\langle {}^{\lambda l}\Psi_-(E_2,E-E_1)\left|r\right|\Phi_{\rm gnd}\rangle\right|^2. \tag{3.38}$$

In 1970, Burke and co-workers[36] introduced the idea of using pseudostates to represent the two-electron continuum channels at energies where they are open in electron-hydrogen scattering. While they only used this representation to approximate the coupling of the $2e^-$ continuum to the $1s$-to-$2s$ and $1s$-to-$2p$ excitation channels, we propose to approximate the cross section into that continuum with pseudostates, in a manner which systemizes the recent exploratory work of Gallaher.[37]

If we could express the remaining integral over dE_2 in Eq. (3.38) as a Gaussian quadrature with abscissas at just the points $E_2=\epsilon_{\nu\lambda}$, we could obtain

$$\sigma^{2e^-}_{\rm length}(E)\simeq\frac{4\pi^2\omega}{c}\sum_{\nu\lambda l}^{0<\epsilon_{\nu\lambda}<E/2}(w^{\rm eq})^{N_\lambda}_\nu\times\left|\langle {}^{\lambda l}\Psi_-(\epsilon_{\nu\lambda},E-\epsilon_{\nu\lambda})\left|r\right|\Phi_{\rm gnd}\rangle\right|^2, \tag{3.39}$$

where the equivalent weight $(w^{\rm eq})^{N_\lambda}_\nu$ is defined as the usual quadrature weight divided by the weight function evaluated at the abscissa.[30,31] Recent work by Yamani and Reinhardt[31] has demonstrated that diagonalizing the hydrogen-atom Hamiltonian in accordance with Eq. (2.10), in the Laguerre basis of Eq. (2.12), giving abscissas $\epsilon_{\nu\lambda}$, indeed generates a Gauss quadrature, of a modified Pollaczek form. Moreover, they have shown that the equivalent weights $(w^{\rm eq})^{N_\lambda}_\nu$ provide just the multiplicative factor needed to convert a δ-function-normalized continuum wave function into a unit-normalized pseudostate.[31] Thus, extending their

single-electron argument, we obtain an approximation for the two-electron cross section in terms of pseudostates:

$$\sigma^{2e^-}_{\text{length}}(E) \simeq \frac{4\pi^2\omega}{c} \sum_{\Gamma}^{0<\epsilon_{\nu\lambda}<E/2} |\langle {}^{\Gamma}\Theta_-(E)|r|\Phi_{\text{gnd}}\rangle|^2. \tag{3.40}$$

At energies just above 0, where only a few terms are included in the sum, Burke and Mitchell[36] have noted that an approximation such as Eq. (3.40) cannot be expected to give a smooth cross section, but as soon as a moderate number of pseudostates are used, the approximation should improve and give a reasonable picture of the average energy dependence of the cross section.

The inequivalent treatment of the two free electrons is not unreasonable in that by taking the energy of the free electron, E_1, greater than the energy of the hydrogen-atom pseudostate, E_2, we have implicitly chosen a model where the electron with greater energy feels a screened Coulomb potential which eventually goes to zero faster than $1/r^2$, while the electron with lesser energy feels the full unscreened long-range attraction of the nucleus.

IV. COMPUTATIONAL DETAILS

To form the partial photodetachment cross sections into the various open channels in accordance with Eq. (3.33), it is necessary to calculate the ground-state wave function for H^-, the scattering wave function for the channel of interest, and the dipole matrix element between the two. A modified version of the configuration-interaction (CI) program written by Schaefer[38] with $8s$, $6p$, and $4d$ Slater-type atomic orbitals combined into 67 ${}^1S$ two-electron configurations was used to approximate the wave function for the H^- ground state. Optimization of the exponents of the Slater orbitals yielded an energy of $-0.527\,38$ a.u. to be compared with an accurate value of $-0.527\,751$ from an extensive Pekeris calculation.[39]

As indicated in the theory in Secs. II and III, several steps are required in the formation of the scattering state, ${}^{\Gamma}\Theta_-(E)$. The most efficient method involves performing as many steps as possible before designating a total energy E. First, the full Hamiltonian was formed and diagonalized in the inner basis functions Φ_i of Eqs. (3.1) and (3.30) either by the Schaefer program or by a two-electron Laguerre-function CI. Basis sets as large as $10s$, $10p$, and $6d$ orbitals of the form Eq. (2.13) were combined to give, in this case, 160 configurations and 36 approximate scattering channels. A variety of exponents ξ_l were used. In what follows, the abbreviated notation of $10s10p6d(2,1,3)$ will be used to indicate a full ${}^1P$ CI generated by taking all ${}^1P^o$ configurations arising from $10s$, $10p$, and $6d$ orbitals with the exponents, $\xi_s = 2$, $\xi_p = 1$, and $\xi_d = 3$.

In addition to diagonalizing the full Hamiltonian in the inner basis, the dipole moments P_Γ of the basis functions, both inner and outer, with the ground state can be calculated independent of the total energy. If we designate for the inner functions

$$P^{\text{inner}}_{\Gamma} = \langle \Theta^{\text{inner}}_{\Gamma} | r | \Phi_{\text{gnd}} \rangle, \tag{4.1}$$

then by Eqs. (3.30)–(3.32), we can write

$$P^{\text{inner}}_{\Gamma} = +\frac{1}{\pi} \sum_{\Gamma''} \sum_{k} \frac{DM_k (DU)^{\Gamma''}_k}{E_k - E} k(\overline{W}CJC)^{-1}_{\Gamma\Gamma''}, \tag{4.2}$$

where

$$DM_k = \sum_i \langle \Phi_i | r | \Phi_{\text{gnd}} \rangle U_{ik}. \tag{4.3}$$

The individual elements in the sum (4.3) were calculated by decomposing both Φ_{gnd} and Φ_i into Slater functions to do the radial integrals, and then transforming to integrals over configurations. Similar to Eq. (4.1), we can designate

$$P^{\text{outer}}_{\Gamma} = \sum_{n'=N^0_l} \langle \Phi^{\Gamma'}_{n'} | r | \Phi_{\text{gnd}} \rangle f^{\Gamma'\Gamma}_{n'} \tag{4.4}$$

for the outer functions defined in Eq. (2.14). Since the transformation from the outer basis functions $\Phi^l_{n'}$ to Slater functions involves so many terms for high n that roundoff error becomes a problem, it was necessary to do some of the radial integrals directly over the Φ^l_n and the Φ^l_n and the Slater functions of the ground state. The total dipole moment with the scattering wave function, in the standing-wave form, Θ_Γ is clearly the sum of $P^{\text{inner}}_{\Gamma}$ and $P^{\text{outer}}_{\Gamma}$.

As mentioned with Eq. (3.29), the elements $(DU)^{\Gamma}_i$ can be formed independent of the energy. Thus having calculated dipole elements over the basis functions outlined above and having fromed $(\text{DU})^{\Gamma}_i$, it is not necessary to retain the full matrix of eigenvectors U_{ik}, produced by the CI. This involves a considerable savings in core storage space.

Once these energy-independent steps are carried out, the theory delineated in Sec. III was followed straightforwardly to the $\overline{W}$ matrix of Eq. (3.24) to the reactance matrix of Eq. (3.21) and the final scattering cross sections of Eq. (3.33). The matrix inversions necessitated by Eqs. (3.21) and (3.34) were carried out by Gauss elimination. Table I shows the channels, including the target-state designation, target energy, and angular momentum

TABLE I. List of the 36 channels incorporated in the $10s10p6d$ (2, 1, 3) calculation. The channel number is given in column 1, the principal quantum number and angular momentum of the target in column 2, the angular momentum of the outgoing free electron in column 3, and the energy of the target pseudostate in column 4. The channels have been numbered in order of increasing target energy.

Channel	Target	Wave	Target energy
1	$1s$	p	$-5.000\,000\times10^{-1}$
2	$2p$	d	$-1.250\,000\times10^{-1}$
3	$2p$	s	$-1.250\,000\times10^{-1}$
4	$2s$	p	$-1.249\,991\times10^{-1}$
5	$3p$	d	$-5.555\,556\times10^{-2}$
6	$3p$	s	$-5.555\,556\times10^{-2}$
7	$3s$	p	$-5.282\,436\times10^{-2}$
8	$4p$	d	$-3.121\,078\times10^{-2}$
9	$4p$	s	$-3.121\,078\times10^{-2}$
10	$3d$	p	$-2.817\,459\times10^{-2}$
11	$5p$	d	$-1.728\,078\times10^{-2}$
12	$5p$	s	$-1.728\,078\times10^{-2}$
13	$6p$	d	$3.285\,914\times10^{-3}$
14	$6p$	s	$3.285\,914\times10^{-3}$
15	$4s$	p	$6.352\,175\times10^{-3}$
16	$7p$	d	$4.083\,160\times10^{-2}$
17	$7p$	s	$4.083\,160\times10^{-2}$
18	$8p$	d	$1.119\,000\times10^{-1}$
19	$8p$	s	$1.119\,000\times10^{-1}$
20	$5s$	p	$1.144\,952\times10^{-1}$
21	$4d$	p	$1.450\,721\times10^{-1}$
22	$9p$	d	$2.630\,222\times10^{-1}$
23	$9p$	s	$2.630\,222\times10^{-1}$
24	$6s$	p	$3.116\,350\times10^{-1}$
25	$5d$	p	$4.962\,746\times10^{-1}$
26	$10p$	d	$6.651\,157\times10^{-1}$
27	$10p$	s	$6.651\,157\times10^{-1}$
28	$7s$	p	$6.944\,732\times10^{-1}$
29	$6d$	p	$1.213\,151\times10^{0}$
30	$8s$	p	$1.555\,457\times10^{0}$
31	$11p$	d	$2.394\,892\times10^{0}$
32	$11p$	s	$2.394\,892\times10^{0}$
33	$7d$	p	$2.909\,449\times10^{0}$
34	$9s$	p	$4.121\,219\times10^{0}$
35	$8d$	p	$8.657\,085\times10^{0}$
36	$10s$	p	$1.887\,419\times10$

of the outgoing free electron, for the largest calculation, $10s10p6d(2, 1, 3)$.

V. RESULTS AND DISCUSSION

A. Overview

Total and partial photodetachment cross sections of H^- resulting from the $10s10p6d(2, 1, 3)$ calculation are depicted in Fig. 1 for total energies from −0.5 to 1.2 a.u. With a ground state energy of −0.527 38 a.u., this corresponds to a range in

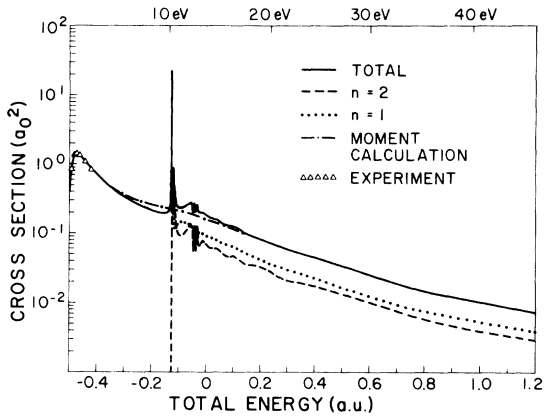

FIG. 1. Photodetachment cross section of H^- from total energy of − 0.5 to 1.2 a.u. Results from the $10s10p6d(2, 1, 3)$ calculation with the length form of the dipole moment are plotted. The solid line gives the total cross section, while the dotted and dashed lines give the partial cross sections for production of H(1s) and H($n = 2$), respectively. The sharp spike in the total cross section at ~ − 0.125 a.u. rising to $21.7a_0^2$ is a Feshbach resonance, while the next, lower, peak at − 0.119 a.u. is the ^1P shape resonance. As discussed in Sec. V D these resonances appear at slightly higher energies, and are somewhat broader than expected owing to the compact basis used in this particular calculation. See Figs. 5, 6, and 7. The structure between − 0.0556 and 0 is indicative of the existence of resonances at thresholds for which $n \geq 3$. The alternately dashed, dotted curve portrays the results of a previously reported (Ref. 21) moment calculation of the *total* cross section, which is seen to give an excellent *average* representation of the cross section. The open triangles near the maximum in the cross section are the relative experimental results of Smith and Burch (Ref. 1) normalized to the present results at 528.0 nm.

the wavelength of the photon from 1664 to 26.4 nm. It is natural to discuss the cross section in Fig. 1 in terms of three energy domains.

In the elastic region, from −0.5 to −0.125 a.u., where H(1s) is the only allowed final state, the cross section is well converged. As shown in Tabel II, the agreement among five different calculations, $7s10p6d(1.5, 1, 3)$, $7s10p6d(2, 1, 3)$, $10s10p6d(2, 1, 3)$, $10s10p6d(0.5, 0.5, 0.5)$, and $7s10p6d4f(2, 1, 3, 3)$, using the length form of the dipole moment [Eq. (3.35b)] is better than 1%, while the difference between them and the $10s10p6d(2, 1, 3)$ velocity-form calculation [Eq. (3.35a)] is no more than 2%. The open triangles in Fig. 1 are the relative experimental values of Smith and Burch[1] in the optical region of the spectrum, normalized to the theoretical results at their standard wavelength of 528.0 nm ($E = -0.4411$ a.u.). At this wavelength the absolute cross section of Geltman,[2(a)] and Branscomb and Smith[2(b)] is 3.28×10^{-17}

TABLE II. Total H^- photoabsorption cross section (a_0^2) in the region from −0.5 to −0.125 a.u. (total energy), where H(1s) is the only energetically accessible state. Results for six different ^1P basis sets are shown for CI using s, p, d, and f atomic functions. Full configuration interaction was carried out for each of the bases shown. The $10s10p6d$ calculations with $\xi_s = \xi_p = \xi_d = 0.5$ were performed in a study of the diffuse resonances near the $n = 2$ threshold: the fact that the cross section only changes a few percent with the introduction of this highly diffuse basis is a good measure of convergence.

Total energy	$7s10p6d$ (1.5, 1, 3) (length)	$7s10p6d$ (2, 1, 3) (length)	$7s10p6d4f$ (2, 1, 3, 4) (length)	$10s10p6d$ (2, 1, 3) (length)[a]	$10s10p6d$ (2, 1, 3) (velocity)[a]	$10s10p6d$ (0.5, 0.5, 0.5) (length)
−0.49	0.994 6	0.999 26	1.000 3	0.999 29	1.018 5	0.976 68
−0.48	1.421 7	1.422 8	1.424 9	1.422 0	1.387 3	1.464 8
−0.47	1.412 8	1.413 0	1.415 2	1.412 7	1.389 6	1.403 1
−0.46	1.342 4	1.342 3	1.344 5	1.342 5	1.342 5	1.353 6
−0.45	1.183 3	1.182 9	1.184 6	1.183 2	1.189 5	1.175 4
−0.40	0.708 23	0.708 22	0.708 63	0.708 20	0.705 90	0.728 31
−0.35	0.468 27	0.468 33	0.467 91	0.468 14	0.466 89	0.467 39
−0.30	0.339 65	0.340 04	0.339 34	0.339 76	0.334 91	0.335 74
−0.25	0.260 24	0.260 45	0.259 59	0.260 38	0.256 21	0.255 42
−0.20	0.211 09	0.210 84	0.210 02	0.211 13	0.209 24	0.207 98
−0.15	0.193 96	0.192 35	0.191 56	0.193 93	0.193 63	0.193 02

[a] These calculations differ only in the method of evaluating the dipole moment, length, or velocity.

cm^2 ±~10%. The $10s10p6d$ calculation gives 3.019×10^{-17} cm^2 ($1.0788a_0^2$) in the length approximation, and 3.024×10^{-17} cm^2 ($1.0806a_0^2$) in the velocity approximation. These results may be compared with 3.06×10^{-17} cm^2 (length) and 3.01×10^{-17} cm^2 (velocity) of Ajmera and Chung,[19] 3.01×10^{-17} cm^2 of Kim[16] (via a moment technique), 2.96×10^{-17} cm^2 of Doughty *et al.*,[13] and 2.99×10^{-17} cm^2 of Geltman,[2] again at 528.0 nm. All of these results are consistent with the recent absolute measurements of Popp and Kruse.[3]

From the $n = 2$ inelastic threshold at −0.125 through the energies of the $n \geq 3$ Rydberg states of hydrogen up to the two-electron ejection threshold at zero energy the cross section in Fig. 1 exhibits considerable structure. Just below the hy-

TABLE III. Total H^- photoabsorption cross section (a_0^2) above the threshold for two-electron ejection ($E^{tot} > 0$). Results are shown for the same basis sets discussed in Table II. Convergence of the total cross section as calculated from the length and velocity forms is satisfactory. The results for the diffuse basis with $\xi_s = \xi_p = \xi_d = 0.5$ have begun to deteriorate as the basis can represent only very-low-energy excitations in the continuum.

Total energy	$7s10p6d$ (1.5, 1, 3) (length)	$7s10p6d$ (2, 1, 3) (length)	$7s10p6d4f$ (2, 1, 3, 4) (length)	$10s10p6d$ (2, 1, 3) (length)[a]	$10s10p6d$ (2, 1, 3) (velocity)[a]	$10s10p6d$ (0.5, 0.5, 0.5) (length)
0.2	0.083 68	0.083 18	0.083 28	0.083 35	0.081 95	0.098 07
0.4	0.044 00	0.044 29	0.043 91	0.044 45	0.043 93	0.042 97
0.6	0.025 26	0.025 11	0.024 63	0.025 13	0.024 94	0.022 60
0.8	0.014 76	0.014 70	0.014 70	0.014 80	0.014 72	0.015 56
1.0	0.010 15	0.010 09	0.010 01	0.010 13	0.010 13	0.011 57
1.2	0.007 395	0.007 369	0.007 351	0.007 387	0.007 424	0.009 001
1.4	0.005 553	0.005 526	0.005 541	0.005 545	0.005 600	0.007 173
1.6	0.004 185	0.004 167	0.004 180	0.004 180	0.004 233	0.005 810
1.8	0.003 162	0.003 151	0.003 166	0.003 159	0.003 200	0.004 771
2.0	0.002 409	0.002 407	0.002 407	0.002 409	0.002 438	0.003 965

[a] These calculations differ only in the method of evaluating the dipole moment, length, or velocity.

TABLE IV. H^- total photoabsorption cross section as a function of wavelength from 1219 to 18.0 nm in units of 10^{-17} cm^2. Results are not given in the region between $n=2$ and $n=\infty$ where there is considerable resonance structure (see Fig. 2).

Wavelength (nm)	Calculated[a] cross section (10^{-17} cm^2)	Wavelength (nm)	Calculated[a] cross section (10^{-17} cm^2)
1219	2.80	62.6	0.233
962	3.98	49.1	0.124
794	3.95	40.4	0.0703
676	3.76	34.3	0.0414
589	3.31	29.8	0.0283
528	3.02	26.4	0.0206
358	1.98	23.6	0.0155
257	1.31	21.4	0.0117
200	0.951	19.6	0.0088
164	0.729	18.0	0.0067
139	0.591		
121	0.543		

[a]Results are given to three significant figures and are those from the $10s10p6d$ (2, 1, 3) length calculations of Tables II and III.

drogenic $n=2$ threshold there is a sharp peak which we identify as a Feshbach resonance, while the broader feature just above the threshold is the ^1P shape resonance. These resonances are discussed in more detail in Sec. V D. The further structure between the $n=3$ threshold at $-\frac{1}{18}$ a.u. and 0 arises from the pseudostate representation of the rest of the Rydberg series of the residual hydrogen atom. Since, as can be seen from the threshold energies of channels 5–12 in Table I, there are only a few pseudostates in this region, we do not attempt to interpret the oscillations in the calculated cross section but rather accept them as indicative of a more complicated actual threshold and resonance structure. As the $2s$-$2p$ degeneracy, which produces a $1/r^2$ off-diagonal coupling between channels connected to the $2s$ and $2p$ thresholds,[40] was not taken explicitly into account the partial cross section into the $2s$ and $2p$ final states was not well converged.[7] Thus only the cross section for the sum (which *is* well converged) into all $n=2$ states is shown in Fig. 1.

At energies above the threshold for two-electron ejection at $E=0$, the total cross section becomes smoother, and it is again useful to compare the results from the five different calculations as was done in the elastic region in Table II. Table III shows that the five length and one velocity calculations agree with each other to within about 3%. As will be argued in conjunction with the two-electron ejection in Sec. V C, the oscillations in the $n=2$ and total cross section just above $E=0$ are artifacts of the pseudostate approximation.

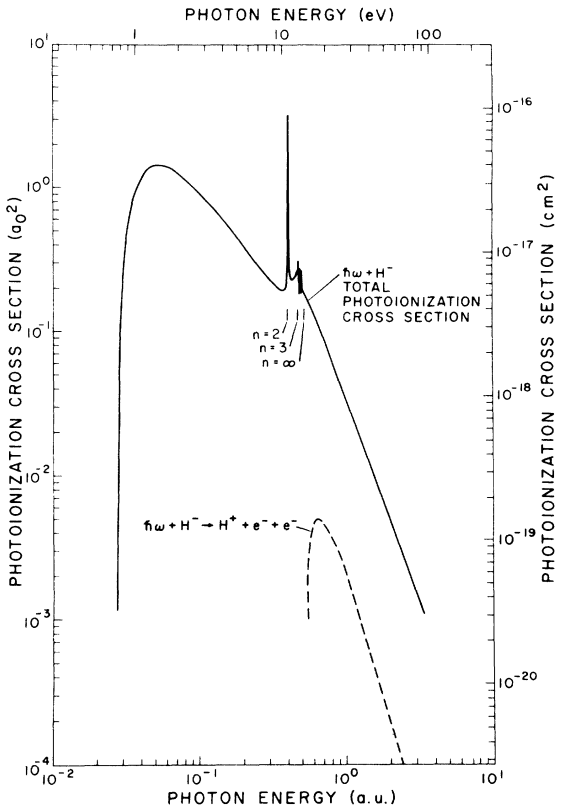

FIG. 2. H^- photodetachment cross section. The total cross section and two-electron ejection cross sections are shown over a wide range of photon energies (in eV and a.u.). The total cross section was obtained from the data of Fig. 1, off resonance, combined with that of Fig. 6 near the thresholds. The Feshbach resonance (Fig. 6) is much too narrow to be seen on this scale. The sharp resonance just above $n=2$ is the ^1P shape resonance discussed in Sec. V D. The two-electron ejection cross section is a smoothed version of that shown in Fig. 4.

The overall results are summarized in Table IV, where the total photoabsorption cross section is given in cm^2 over the range from 1664 to 18.0 nm, and in Fig. 2, which gives a global view of the total and the two-electron ejection cross sections.

B. Elastic threshold behavior

As derived in Sec. 4 of IV, the J-matrix method incorporates the threshold laws of Wigner explicitly.[41] In particular, the photodetachment cross section of a singly charged negative ion is expected to exhibit a dependence on the channel momentum of k_Γ^{2l+1} near $k_\Gamma=0$. For the elastic threshold of H^-, the $1s$ state of H is left behind, and hence the

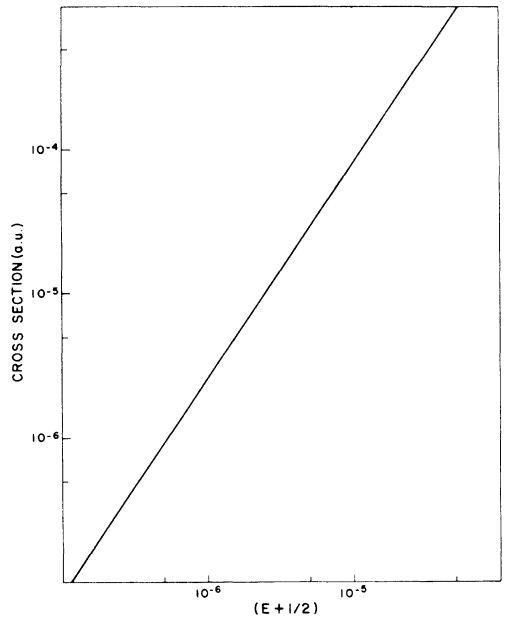

FIG. 3. Total photoionization cross section near the H(1s) threshold. The Wigner threshold laws predict that the cross section should depend on the $\frac{3}{2}$ power of $E+\frac{1}{2}$ near the threshold. The slope of the curve of $\log\sigma$ versus $\log(E+\frac{1}{2})$ in the figure is 1.500 ± 0.0005, consistent with the prediction.

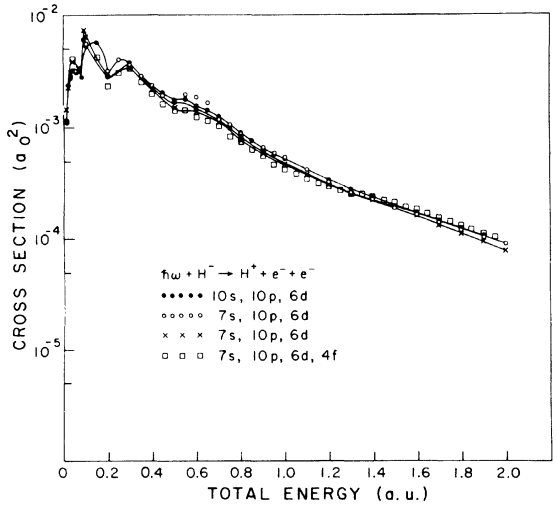

FIG. 4. Cross section for two-electron ejection. Dotted curve denotes the results from the $10s10p6d$ (2, 1, 3) length calculation, a velocity calculation giving the same results to within the scatter. × and ○ depict the results of smaller $7s10p6d$ calculations with exponents (2, 1, 3) and (1.5, 1.3), respectively. □'s indicate the results of a $7s10p6d4f(2,1,3,4)$ calculation carried out to check convergence of the partial-wave expansion. The use of a partial quadrature by pseudostates gives uneven results out to ~0.3 a.u., but after that the cross section is converged to an estimated 15%.

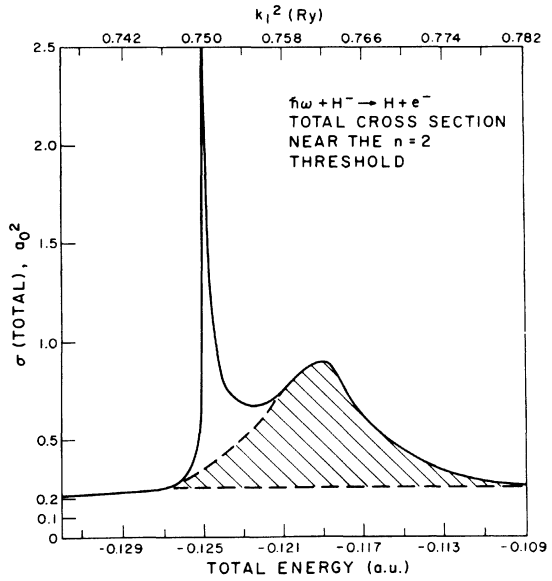

FIG. 5. H^- photodetachment resonance structure in the total cross section near $n=2$, as calculated with the $10s10p6d(2,1,3)$ basis, which is too compact to adequately represent the resonances, as discussed in the text. The shaded area gives an estimate of ~0.03 for the oscillator strength of the ^1P shape resonance, which in this approximation peaks at −0.119 a.u. The oscillator strength estimate follows the technique of Macek (Ref. 48). As can be seen in the figure, separation of the oscillator strength into that "belonging" to the Feshbach and shape resonances is ambiguous but 0.03 would seem to be an overestimate for the shape resonance. k_1^2 gives the energy (in rydbergs) above the hydrogenic ground state.

outgoing electron must be a p wave, and we expect that the cross section will behave as

$$\sigma(E) \rightarrow (k_1)^3 \quad \text{or} \quad \rightarrow (E+\tfrac{1}{2})^{3/2}, \tag{5.1}$$

E being the total energy. In Fig. 3, the logarithm of σ is plotted versus the logarithm of $E+\frac{1}{2}$ for $E+\frac{1}{2}$ from 10^{-7} to 10^{-5}. Consistent with Eq. (5.1), the curve is a straight line with slope 1.500 ± 0.0005.

C. Two-electron ejection

Results of $10s10p6d(2,1,3)$, $7s10p6d(2,1,3)$, $7s10p6d(1.5,1,3)$, and $7s10p6d4f(2,1,3,3)$ calculations of the single-photon two-electron ejection cross section are shown in Fig. 4. As discussed in Sec. III D, the cross section is poorly approximated close to the threshold, from 0 to 0.3 a.u., because of the small number of pseudostates used there in the sum in Eq. (3.40). Higher accuracy could be obtained by using the equivalent weights and pseudochannel cross sections to interpolate a smoothed wave function $^{\lambda I}\Psi_-$ to use in Eq. (3.39),

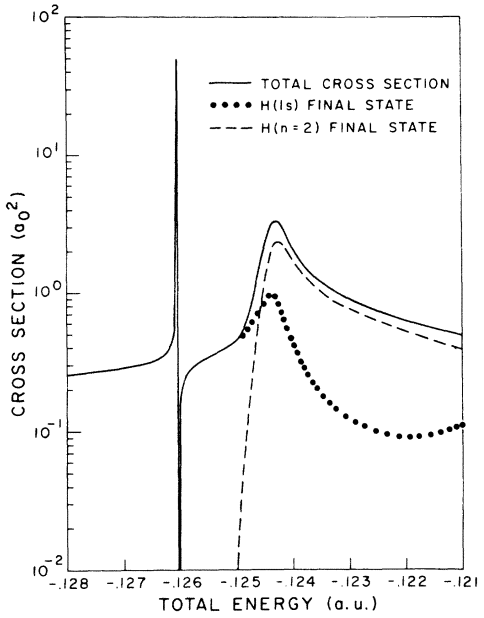

FIG. 6. H^- photodetachment resonance structure near the $n=2$ threshold, as calculated using the $10s10p6d$ (0.5, 0.5, 0.5) basis discussed in the text, giving a very reasonable estimate of the partial and total cross sections in the resonance region.

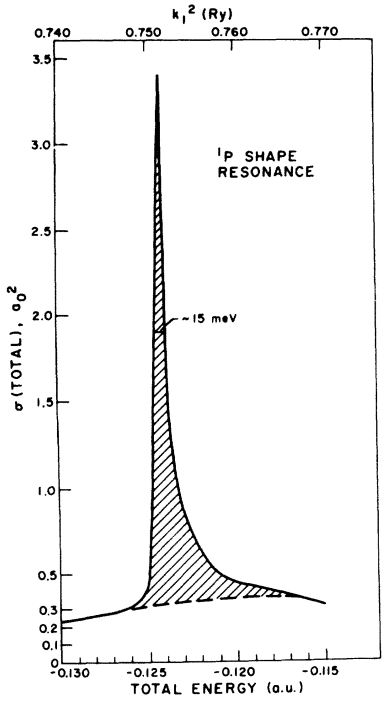

FIG. 7. ^1P shape resonance as seen in the total cross section for photo detachment of H^-, in the $10s10p6d$ (0.5, 0.5, 0.5) calculation. The Feshbach resonance at ~ − 0.126 a.u. has been graphically subtracted out. The shaded area gives an estimated (Ref. 48) oscillator strength of 0.024 ± ~ 15%, in comparison to the three-state close-coupling estimate of 0.044. k_1^2 gives the energy (in rydbergs) above the hydrogenic ground state.

but the predictions of Wannier[42] imply that near $E=0$ a very large number of partial waves are needed to describe the highly correlated long-range interaction between the slowly moving electrons. In our s, p, d calculations, we can only note that the d wave dominates from 0 to 0.6 a.u., consistent with this expectation. Above $E=0.3$, however, all five calculations give a smooth cross section for two-electron ejection in agreement with each other to an estimated 15%. To our knowledge, there are no measurements of this cross section. In Fig. 2 it is seen that over the photon energy range from 20 to 100 eV $\sigma_{2e}/\sigma_{tot} \sim 4\%$, in qualitative agreement with the same ratio in He.[43]

D. Resonance structure near the $n=2$ threshold

The majority of the calculations were carried out with a tightly correlated basis with exponents of order $1a_0^{-1}$ to $3a_0^{-1}$. These exponents give a well-converged nonresonant cross section, but are too compact to give a good representation of the diffuse resonances near the hydrogenic $n=2$ threshold and totally incapable of representing the very diffuse[44] resonances near the higher thresholds. The problems encountered are shown in Fig. 5, where the resonance structure near the $n=2$ threshold (at −0.125 a.u.) is shown as calculated using the $10s10p6d(2, 1, 3)$ basis discussed earlier. The lowest ^1P Feshbach resonance appears at −0.125 a.u. rather than at −0.126 a.u. as expected. The "shape" resonance, rising to a height of $0.89a_0^2$ at −0.119 a.u. with a roughly estimated full width at half-maximum (FWHM) of 4×10^{-3} a.u., is similarly misplaced and too broad: The close-coupling plus correlation e-H scattering calculations of Taylor and Burke[45] as analyzed by Macek and Burke[6] would lead us to expect a much narrower ($\sim 5\times10^{-4}$ a.u.) shape resonance occurring at an energy of ~−0.124 34 a.u.

Scaling estimates based on independent[46] Laguerre-CI work within a Feshbach projection scheme suggested that the exponent choice $\xi=0.5$ would be more suitable for obtaining a good "position" for the lowest ^1P Feshbach resonance. This choice of scale parameter, with the fairly large radial basis sets used, also allows spanning of the hyperspherical "potential curves" of Lin,[9] which give rise to the Feshbach and shape resonances. The results of a single $10s10p6d(0.5, 0.5, 0.5)$ calculation are shown in Fig. 6. The lowest ^1P Feshbach resonance has a minimum at −0.126 019 a.u., in good agreement with previous values.[47] The shape resonance now peaks ~18 meV above the $n=2$ threshold with a width (FWHM) of $\Gamma \sim 15$ meV, in

excellent agreement with the e-H scattering estimates.[6] However the peak height is 9.5×10^{-17} cm^2 ($3.4a_0^2$) in contrast to the Macek "equal-area" estimate[5] of 15×10^{-17} cm^2. Estimates of the oscillator strength (see Figs. 5 and 7) following the technique of Macek[48] yielded ~0.03 (quite uncertain, but undoubtedly an overestimate) for the $10s10p6d(2,1,3)$ calculation and 0.024 (±15%) for the $10s10p6d(0.5,0.5,0.5)$ calculation. These are to be compared with the Macek[5] and Hyman *et al.*[7] $1s$-$2s$-$2p$ close-coupling estimate of 0.044, which Macek assumed would not change appreciably with the addition of correlation terms (closed channels). At this point we note only that these results suggest that the Macek oscillator strength and peak height for the ^1P shape resonance may be too large by a factor of ~2, possibly helping to rationalize the negative results of Ott *et al.*[4]

ACKNOWLEDGMENTS

Helpful conversations with J. Slater, J. Cooper, J. R. Taylor, D. Truhlar, and J. Macek are gratefully acknowledged. J. T. B. acknowledges the support of the Veteran's Administration, use of a dipole-matrix code written by S. V. ONeil, and the general computational assistance of S. V. ONeil, C. Kunasz, and U. Palmer. W.P.R. acknowledges the hospitality of the Aspen Center for Physics where a final draft of the manuscript was prepared. This work was partially supported by the NSF under Grant MPS74-19605.

---

*On leave from Dept. of Chemistry, Harvard University, Cambridge, Mass. 02138. **Present address:** Fakultät für Chemie, Universität Bielefeld, 48 Bielefeld, Postfach 8640, West Germany.

†Camille and Henry Dreyfus Teacher-Scholar.

[1]S. J. Smith and D. S. Burch, Phys. Rev. 116, 1125 (1959).

[2](a) S. Geltman, Astrophys. J. 136, 935 (1962); (b) L. M. Branscomb and S. J. Smith, Phys. Rev. 98, 1028 (1955).

[3]H.-P. Popp and S. Kruse, J. Quant. Spectrosc. Radiat. Transfer 16, 683 (1976).

[4]W. R. Ott, J. Slater, J. Cooper, and G. Gieres, Phys. Rev. A 12, 2009 (1975).

[5]J. Macek, Proc. Phys. Soc. Lond. 92, 365 (1967).

[6]J. Macek and P. G. Burke, Proc. Phys. Soc. Lond. 92, 351 (1967).

[7]H. A. Hyman, V. L. Jacobs, and P. G. Burke, J. Phys. B 5, 2282 (1972).

[8](a) D. Herrick and O. Sinanoğlu, Phys. Rev. A 11, 97 (1975); (b) C. E. Wulfman, Chem. Phys. Lett. 40, 139 (1976), and references therein.

[9]C. D. Lin, Phys. Rev. Lett. 35, 1150 (1975); Phys. Rev. A 14, 30 (1976).

[10]J. W. McGowan, J. F. Williams, and F. K. Carley, Phys. Rev. 180, 132 (1969).

[11]F. Williams and B. A. Willis, J. Phys. B 7, L61 (1974).

[12]S. Chandrasekhar, Astrophys. J. 102, 223 (1945); 102, 395 (1945).

[13]N. A. Doughty, P. A. Fraser, and R. P. McEachran, Mon. Not. R. Astron. Soc. 132, 255 (1966).

[14]K. L. Bell and A. E. Kingston, Proc. Phys. Soc. Lond. 90, 895 (1967).

[15]S. A. Adelman, Phys. Rev. A 5, 508 (1972).

[16]Y.-K. Kim, Argonne National Laboratory Report No. ANL 7220 p. 30, 1966–67 (unpublished); M. Inokuti and Y.-K. Kim, Phys. Rev. 173, 154 (1968).

[17]P. W. Langhoff and C. T. Corcoran, J. Chem. Phys. 61, 146 (1974).

[18]T. N. Rescigno, C. W. McCurdy, Jr., and V. McKoy, J. Chem. Phys. 64, 477 (1976).

[19]M. P. Ajmera and K. T. Chung, Phys. Rev. A 12, 475 (1975).

[20]P. W. Langhoff, C. T. Corcoran, J. S. Sims, F. Weinhold, and R. M. Glover, Phys. Rev. A 14, 1042 (1976).

[21]J. T. Broad and W. P. Reinhardt, Chem. Phys. Lett. 37, 212 (1976).

[22]S. J. Risley, in *Atomic Physics IV. Proceedings of the Fourth International Conference on Atomic Physics, 1974*, edited by G. Zu Putlitz, E. W. Weber and A. Winnacker (Plenum, New York, 1975).

[23]E. J. Heller and H. A. Yamani, Phys. Rev. A 9, 1201 (1974).

[24]E. J. Heller and H. A. Yamani, Phys. Rev. A 9, 1209 (1974).

[25]H. A. Yamani and L. Fishman, J. Math. Phys. 11, 410 (1975).

[26]E. J. Heller, Phys. Rev. A 12, 1222 (1975).

[27]J. T. Broad and W. P. Reinhardt, J. Phys. B 9, 1491 (1976).

[28]See, for example, K. Smith, *The Calculation of Atomic Collision Processes* (Wiley-Interscience, New York, 1971); P. G. Burke and K. Smith, Rev. Mod. Phys. 34, 458 (1962); P. G. Burke and W. D. Robb, Adv. At. Mol. Phys. 11, 143 (1975).

[29]J. R. Taylor, *Scattering Theory* (Wiley, New York, 1974).

[30]E. J. Heller, W. P. Reinhardt, and H. A. Yamani, J. Comput. Phys. 13, 536 (1973).

[31]H. A. Yamani and W. P. Reinhardt, Phys. Rev. A 11, 1144 (1975).

[32]R. J. Damburg and S. Geltman, Phys. Rev. Lett. 20, 485 (1968).

[33]E. P. Wigner, Phys. Rev. 73, 1002 (1948).

[34]P. G. Burke and W. D. Robb, Ref. 28.

[35]R. J. W. Henry and L. Lipsky, Phys. Rev. 153, 51 (1967).

[36]P. G. Burke and J. F. B. Mitchell, J. Phys. B 6, 320 (1973); P. G. Burke and T. G. Webb, J. Phys. B 3, L131 (1970).

[37]D. F. Gallaher, J. Phys. B 7, 362 (1974).

[38]H. F. Schaefer, thesis (Stanford University, 1969) (unpublished).

[39]P. K. Kabir and E. E. Salpeter, Phys. Rev. 108, 1256

(1957).
[40]M. Gailitis and R. Damburg, Proc. R. Soc. Lond. 82, 192 (1963); see also the discussion in K. Smith, Ref. 28.
[41]E. Wigner, Phys. Rev. 73, 1002 (1948).
[42]G. H. Wannier, Phys. Rev. 90, 817 (1953); U. Fano, Comments At. Mol. Phys. 1, 159 (1970); J. Phys. B 7, L401 (1974).
[43]V. Schmidt, N. Sandner, and H. Kuntzemüller, Phys. Rev. A 13, 1743 (1976); V. Schmidt, N. Sandner, H. Kuntzemüller, P. Dhez, F. Wuillenmier, and E. Källe, LURE Report 75/03, Universite Paris–Sud, Orsay, France (unpublished); and Phys. Rev. A 13, 1748 (1976).
[44]J. C. Y. Chen, Phys. Rev. 156, 150 (1967).
[45]A. Taylor and P. G. Burke, Proc. Phys. Soc. Lond. 92, 336 (1967).
[46]W. P. Reinhardt (unpublished work).
[47]O'Malley and Geltman [T. F. O'Malley and S. Geltman, Phys. Rev. 137, A1344 (1965)] give – 0.125 965 a.u., and Ajmera and Chung [M. P. Ajmera and K. T. Chung, Phys. Rev. A 10, 1013 (1974)] give values of – 0.125 973 and – 0.125 995 from successively larger Hylleraas type calculations.
[48]The area under the curve is computed in units of (a_0^2) × (rydbergs) and multiplied by $(4\pi^2 a_0^2 \alpha)^{-1}$ where, in atomic units, $\alpha = e^2/\hbar c = 1/c \cong \frac{1}{137}$ and $a_0 = 1$; see Ref. 5.